

Docking of the alkaloid geissospermine into acetylcholinesterase: a natural scaffold targeting the treatment of Alzheimer's disease

Jocley Queiroz Araújo · Josélia Alencar Lima ·
Angelo da Cunha Pinto · Ricardo Bicca de Alencastro ·
Magaly Girão Albuquerque

Received: 28 May 2010 / Accepted: 30 August 2010 / Published online: 16 September 2010
© Springer-Verlag 2010

Abstract Pharmacological studies from our group [Lima et al. *Pharmacol Biochem Behav* 92:508, (2009)] revealed that geissospermine (GSP), the major alkaloid of the bark extract of Brazilian *Geissospermum vellosii*, inhibits acetylcholinesterases (AChEs) in the brains of rats and electric eels (*Electrophorus electricus*). However, the binding mode (i.e., conformation and orientation) of this indole-indoline alkaloid into the AChE active site is unknown. Therefore, in order to propose a plausible binding mode between GSP and AChE, which might explain the observed experimental inhibitory activity, we performed comparative automatic molecular docking simulations using the AutoDock and Molegro Virtual Docker (MVD) programs. A sample of ten crystal structures of the Pacific electric ray (*Torpedo californica*)

TcAChE, in complex with ten diverse active site ligands, was selected as a robust re-docking validation test, and also for GSP docking. The MVD results indicate a preferential binding mode between GSP and AChE, in which GSP functional groups may perform specific interactions with residues in the enzyme active site, according to the ligand–protein contacts detected by the LPC/CSU server. Four hydrogen bonds were detected between GSP and Tyr121, Ser122, Ser200, and His440, in which the last two residues belong to the catalytic triad (Ser200···His440···Glu327). Hydrophobic and π – π stacking interactions were also detected between GSP and Phe330 and Trp84, respectively; these are involved in substrate stabilization at the active site. This study provides the basis to propose structural changes to the GSP structure, such as molecular simplification and isosteric replacement, in order to aid the design of new potential AChE inhibitors that are relevant to the treatment of Alzheimer's disease.

Electronic supplementary material The online version of this article (doi:10.1007/s00894-010-0841-2) contains supplementary material, which is available to authorized users.

J. Q. Araújo (✉) · R. B. de Alencastro · M. G. Albuquerque (✉)
Instituto de Química (IQ), Programa de Pós-Graduação em
Química (PPGQu), Laboratório de Modelagem Molecular
(LabMMol), Universidade Federal do Rio de Janeiro (UFRJ),
CT, Bloco A, Sala 609,
Rio de Janeiro, Brazil
e-mail: jocleymol@yahoo.com.br

M. G. Albuquerque
e-mail: magaly@iq.ufrj.br

J. A. Lima · A. C. Pinto
Instituto de Química (IQ), Programa de Pós-Graduação em
Química (PPGQu), Laboratório de Produtos Naturais (Pilab),
Universidade Federal do Rio de Janeiro (UFRJ),
CT, Bloco A, Sala 621,
Rio de Janeiro, Brazil

Keywords Acetylcholinesterase · Alzheimer disease ·
Geissospermine · Indole-indoline alkaloid · Molecular
docking · Molecular modeling

Introduction

Alzheimer's disease (AD) is a neurodegenerative disorder associated with a selective loss of cholinergic neurons in the brain, accompanied by decreasing levels of the neurotransmitter acetylcholine (ACh) [1]. The occurrence of AD correlates with an increase in the accumulation of beta-amyloid-rich senile plaques and neurofibrillary tangles in the brain [2].

The disease is characterized clinically by a progressive decline in cognitive function, executive function losses, and memory deficits, eventually leading to incapacitating dementia before death [3]. AD is associated with risk factors such as increased parental age at time of birth [4], apolipoprotein E [5], head injury [6], diabetes [7], hypertension [8], high cholesterol levels [9], strokes [10], and smoking [11].

The prevalence of AD increases dramatically with age, and doubles every five years after the age of 65 [12]. The disease affects more women than men, probably because women have a higher life expectancy [13, 14]. It has been estimated that 30–50% of individuals in their eighth to ninth decades have some degree of AD [15].

Studies have shown that the life expectancy for patients with AD can reach about 10 years following diagnosis, with considerable variability from one patient to another [16]. In 2006, there were 26.6 million cases of AD in the world, and by 2050, it is predicted that its prevalence will grow fourfold, to 106.8 million, i.e., one in 85 persons worldwide will be living with the disease [17].

There is currently no treatment to cure or stop the progress of AD, but drug therapy may temporarily relieve some of the symptoms. Current AD treatment has largely involved replacing neurotransmitters, mostly according to the “cholinergic hypothesis” [18], which states that decreased cholinergic transmission plays a major role in the expression of cognitive, functional and (possibly) behavioral symptoms in AD [19–22].

Different strategies have been investigated to improve cholinergic neurotransmission, including increasing ACh synthesis, augmenting pre-synaptic ACh release, stimulating cholinergic post-synaptic muscarinic and nicotinic receptors, and reducing ACh synaptic degradation with AChE inhibitors (i.e., AChEIs or anticholinesterase agents). However, except for the use of AChEIs, current data do not support the use of ACh precursors, pre-synaptic releasing agents, or muscarinic agonists, due to their inefficacy and unacceptable side effects [18].

Compounds that increase ACh levels in the brain, thereby facilitating cholinergic neurotransmission through AChE inhibition, are the main pharmacotherapy for AD [23]. Currently, the use of AChEIs and NMDA (*N*-methyl-D-aspartate) receptor antagonists [24] is endorsed as the standard first-line therapy in patients with mild-to-moderate AD [25].

AChE inhibition has beneficial effects on cognitive, functional, and behavioral symptoms of AD [26–28]. Five drugs have been approved by the US Food and Drug Administration (FDA) for AD treatment. Four are AChEIs (Fig. 1)—tacrine (Cognex™, approved in 1993), donepezil (Aricept™, 1996), rivastigmine (Exelon™, 2000), and galantamine (Reminyl™, 2001); the other is a NMDA receptor antagonist, memantine (Namenda™, 2003) [24].

Nowadays, tacrine is rarely used due to its hepatotoxicity (about 50% of patients) [23, 29]. Donepezil and rivastigmine, which are not hepatotoxic, are usually used in the early-to-moderate stages of AD to treat cognitive loss. However, neither of them cures AD, and they often cause some adverse effects [30]. Only galantamine, with its clinically relevant neuroprotective effects, shows promise in the treatment of AD patients, according to the results from Phase II studies [31, 32]. Therefore, because of the bioavailability problems and side effects of current pharmacotherapy, more effective AChEIs to treat AD are urgently required.

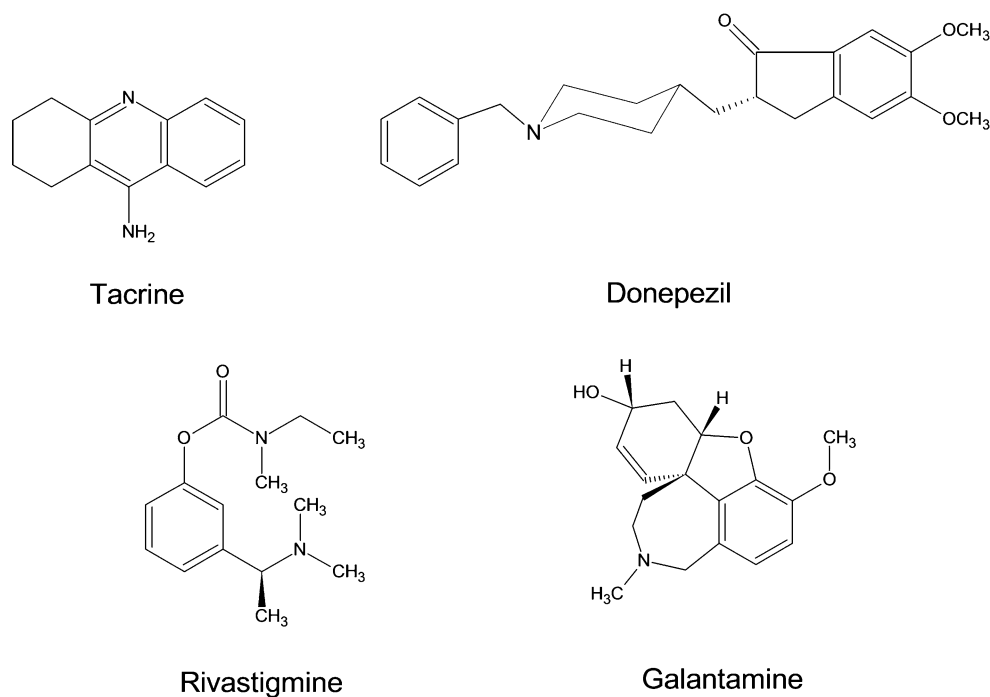
Recently, the anticholinesterase activity of *Geissospermum vellosii*, a Brazilian tree popularly known as Pau-Pereira, was evaluated by our group [J.A. Lima and A.C. Pinto] [33, 34], using Ellman's colorimetric assay in thin-layer chromatography (TLC). These pharmacological studies revealed that in the brains of rats and electric eels (*Electrophorus electricus*), AChEs were inhibited in a concentration-dependent manner by a fraction containing the indole-indoline alkaloid geissospermine (GSP, Fig. 2), which was isolated, identified, and is known to be the major alkaloid of *G. vellosii* stem bark [33, 34]. However, the binding mode (i.e., conformation and orientation) of this alkaloid into the AChE active site is unknown.

The available 3D structures of *Torpedo californica* AChE (*TcAChE*) reveal that the active site is located at the bottom of a narrow cavity about 20 Å deep termed the aromatic gorge, as more than 50% of its amino acids are highly conserved aromatic residues (i.e., Phe120, Phe288, Phe290, Phe330, Phe331, Trp84, Trp233, Trp279, Trp432, Tyr70, Tyr121, Try130, Try334, and Tyr442) that play functional roles [35].

The active site of the AChE consists of a catalytic triad (CT) composed of Ser200···His440···Glu327 and a catalytic anionic site (CAS) composed of Trp84, Phe330, and Glu199. Additionally, there is a peripheral anionic site (PAS) composed of Asp72, Tyr70, Tyr121, Trp279, and Phe290, located at the gorge entrance [36].

Therefore, in order to propose a plausible binding mode between GSP and AChE which might explain the observed experimental inhibitory activity of the AChE, we performed comparative automatic molecular docking simulations using the AutoDock and Molegro Virtual Docker (MVD) programs. Before this, we also performed a robust re-docking validation test using a set of ten crystal structures of the Pacific electric ray (*Torpedo californica*) AChE in complex with ten diverse active site ligands. This set was chosen in order to span the molecular diversity of the ligands bound to the AChE in terms of number of rotatable bonds and molecular volume. This set of ten *TcAChE* structures was also used for the GSP docking simulations.

Fig. 1 2D chemical structures of the four acetylcholinesterase inhibitors (AChEIs) currently approved by the US Food and Drug Administration (FDA) for the treatment of Alzheimer's disease

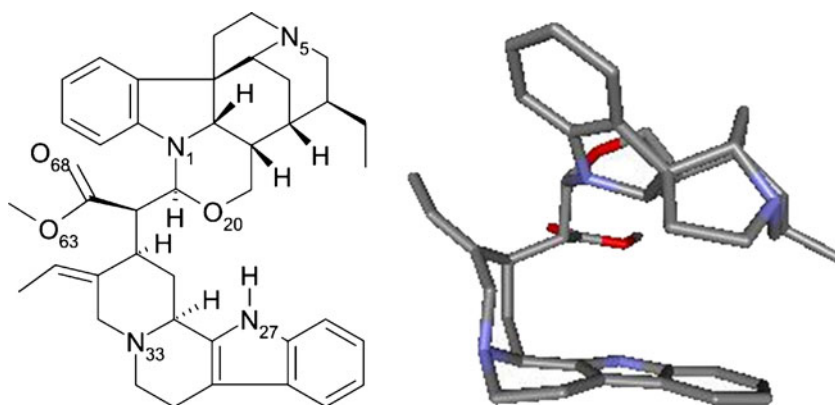


Materials and methods

Protein structures

A set of ten crystal structures of AChEs, in complex with ten diverse active site ligands, was selected as a robust re-docking validation test. The crystal structures of the ten AChE enzymes from the Pacific electric ray (*Torpedo californica*), in complex with their respective ligands, were retrieved from the Protein Data Bank (PDB) [37] at the Research Collaboratory for Structural Bioinformatics (RCSB, <http://www.rcsb.org>). The respective PDB IDs and resolution (R , Å) are: 1ACJ [38] ($R=2.80$), 1ACL [38] ($R=2.80$), 1DX6 [39] ($R=2.30$), 1E3Q [40] ($R=2.85$), 1EVE [41] ($R=2.50$), 1OCE [42] ($R=2.70$), 1U65 [43] ($R=2.61$), 1VOT [44] ($R=2.50$), 2ACE [44] ($R=2.50$), and 2ACK [45] ($R=2.40$).

Fig. 2a-b Chemical structure of the alkaloid geissospermine (GSP). **a** 2D representation. **b** 3D stick model representation of the X-ray diffraction structure of the GSP crystal retrieved from the Cambridge Structural Database (CSD ID: GEISSO10) (colored by element: gray, carbon; blue, nitrogen; red, oxygen)



Ligand structures

The 3D structures of the ten ligands were extracted from their respective complexes with AChE according to the following ligand PDB codes: THA [38] (tacrine), DME [38] (decamethonium ion), GNT [39] ((-)-galantamine), EWB [40] (BW284C51), E20 [41] (E2020), MF2 [42] (MF268), CP0 [43] (CPT-11), HUP [44] ((-)-huperzine A), ACH [44] (acetylcholine), and EDR [45] (edrophonium ion). The chemical 2D structures of all ligands (ACD/Labs software) [46] are shown in Fig. S1 of the “Electronic supplementary material.”

Acetylcholine (ACH) and MF-268 (MF2) are covalently bonded to the enzyme in the structures of complexes 2ACE and 1OCE, respectively. Therefore, in those cases, the covalent bond was broken in order to extract the ligands, and the structures were corrected. In addition, the structure

of MF2 is incomplete, because the whole molecule cleaves during the hydrolysis process.

The 3D structure of GSP alkaloid (CSD ID: GEISSO10) [47] was retrieved from the Cambridge Structural Database (CSD) at the Cambridge Crystallographic Data Centre (CCDC, <http://www.ccdc.cam.ac.uk>) [48].

The ligand atom types and bond orders were corrected manually in the SYBYL v.8.0 program [49]. Hydrogen atoms were added and Gasteiger–Hückel charges were assigned [50]. The geometries of the ligands were optimized for 200 steps with the Simplex algorithm, using the Tripos force field [51], and saved in the SYBYL Mol2 format.

Molecular docking

The docking of ten ligands and the GSP alkaloid into the active site of AChE was performed using the AutoDock v.4.0 [52] and Molegro Virtual Docker (MVD) v.2008.2.4 (Molegro ApS) programs [53]. In order to compare the results from both docking protocols, water molecules, co-factors, and ions were excluded; the protonation states (ligands and protein) were set to the physiological pH; the rotatable bonds of the ligands were set to be free; and the enzyme was treated as a rigid body.

Molecular docking using AutoDock

AutoDock combines a rapid energy evaluation through pre-calculated grids of affinity potentials with a variety of

search algorithms to find suitable binding positions for a ligand on a given macromolecule [54].

The polar hydrogen atoms of the enzymes were added, the non-polar hydrogen atoms were merged, Kollman charges were assigned, and solvation parameters were added. For all ligands, including GSP, the non-polar hydrogen atoms were merged, and the Gasteiger charges were assigned.

The auxiliary program AutoGrid generated the grid maps. The grids, one for each atom type in the ligands, plus one for the electrostatic interactions, were chosen so as to be sufficiently large to include the active site of AChE, since all ligands are bonded within the active site. The grid box dimensions were $60 \times 60 \times 60$ Å around the active site and the grid spacing was set to 0.375 Å. The starting positions of all ligands were outside the grid box (>20 Å away from the center of the binding pocket).

Docking was performed using the empirical free energy function together with the Lamarckian genetic algorithm (LGA) [55]. The LGA protocol applied a population size of 150 individuals, while 250,000 energy evaluations were used for the 100 LGA runs. In addition, the maximum number of evaluations was set to 27,000; the mutation rate to 0.02; the crossover rate to 0.8; and the elitism rate to 1.0.

Clustering histogram analyses were performed after docking searches. Sets of 100 solutions were clustered into groups with a root-mean-square deviation (RMSD) of no more than 1.0 Å. The best conformations were chosen from the lowest docked energy solutions in the cluster populated by the highest number of conformations.

Table 1 Ligand/AChE complex PDB codes and corresponding resolutions (*R*, Å), ligand PDB codes, number of rotatable bonds (nRotB), molecular weight (MW, g mol⁻¹), CPK volume (CPK Vol, Å³), and

RMSD (Å) values obtained from the re-docking validation test performed using the AutoDock and Molegro Virtual Docker (MVD) programs

PDB ID	R	Ligand	nRotB	MW	CPK Vol	RMSD ^c	
						AutoDock	MVD
1ACJ	2.80	THA	0	199.28	217.88	<i>0.58</i>	<i>0.51</i>
1VOT	2.50	HUP	1	243.33	261.14	1.78	<i>0.67</i>
1DX6	2.30	GNT	1	287.36	300.26	<i>0.68</i>	<i>0.65</i>
2ACK	2.40	EDR	2	166.24	196.19	4.94	<i>0.84</i>
2ACE ^a	2.50	ACH	4	146.21	174.47	4.43	1.14
1EVE	2.50	E20	6	380.51	417.25	1.85	<i>0.79</i>
1U65	2.61	CP0	6	587.70	604.59	1.57	1.55
1OCE ^b	2.70	MF2	10	270.42	322.46	4.77	4.91
1ACL	2.80	DME	11	258.49	339.45	3.57	2.64
1E3Q	2.85	EBW	12	406.61	483.34	3.31	3.01

^a In the X-ray structure (2ACE), the natural substrate (acetylcholine, in an all-*trans* conformation) was manually docked into the active site and covalently bound to catalytic serine (Ser200) in a tetrahedral intermediate conformation (the acetylcholine is a model; it is not derived from the experimental data)

^b In the X-ray structure (1OCE), the dimethylmorpholinooctylcarbamate moiety of MF268 is covalently bound to Ser200

^c Italicized RMSD values indicate the best results according to the text

The best docking complex solutions (poses) were analyzed according to the potential intermolecular interactions (ligand/enzyme)—such as hydrogen bonding (H-bonding), cation- π , π - π stacking, hydrophobic, and van der Waals (vdW)—using the LPC/CSU server, which is used to analyze ligand-protein contacts on PDB files [56]. This software automatically classifies the ligand/protein atom types, calculates all atomic contacts and solvent-accessible surfaces for every atom of the ligand in its complex and uncomplexed forms, and determines the contacting residues and types of interactions they can undergo (e.g., hydrogen bonds, hydrophobic-hydrophobic, aromatic-aromatic, aromatic-polar, etc.).

Using the output from the LPC server, we cross-checked the interaction types and refined the results in order to reduce the number of contacts reported by the program. However, it is important to take care when analyzing these potential interactions further, as empirical force fields are generally not parameterized to compute some interactions such as hydrophobic, π - π stacking, and cation- π .

Molecular docking using the Molegro Virtual Docker

The Molegro Virtual Docker (MVD) is based on a new heuristic search algorithm that combines differential evolution with a cavity prediction algorithm. Differential evolution [57] has been successfully applied to molecular docking [58]. During the search process, fast and accurate identification of the potential binding modes is achieved through the use of predicted cavities.

The atom types and the bond orders were corrected to both ligand and enzyme structures using the MVD automatic preparation function. For each complex, the

hydrogen atoms were added and the MVD default charges were assigned.

Potential binding sites (cavities) were detected using the grid-based cavity prediction algorithm. The population size, maximum interactions, scaling factor, and crossover rate were set to 150, 2000, 0.50, and 0.90, respectively. For each complex, we performed 100 independent runs with the MolDock optimizer algorithm, with each run returning one solution (pose).

The highest ranked solution was compared with the known experimental structure (X-ray) in terms of RMSD, and similar poses were clustered within a RMSD of 1.00 Å. The MolDock score function with a grid resolution of 0.30 Å was used to precompute score grids for rapid dock evaluation. Guided differential evolution and a force-field-based docking scoring function were used to search for the binding orientation and conformation of each candidate molecule.

In a similar manner to AutoDock, the best docking complex solutions were analyzed according to the potential intermolecular interactions (ligand/enzyme) using the LPC/CSU server [56].

Results and discussion

Validation of the docking protocols by re-docking using the ten ligand/AChE complexes

Before docking GSP into the ten AChE structures, the AutoDock and MVD docking protocols were validated using the ten ligand/AChE complexes selected from PDB: THA/1ACJ; DME/1ACL; GNT/1DX6; EBW/1E3Q; E20/

Fig. 3 The superpositions of the best docked poses of CP0 (AutoDock, RMSD=1.57 Å and MVD, RMSD=1.55 Å) and DME (AutoDock, RMSD=3.57 Å and MVD, RMSD=2.64 Å) (stick model colored by element) with the corresponding bounded X-ray conformation (light gray in AutoDock and green in MVD)

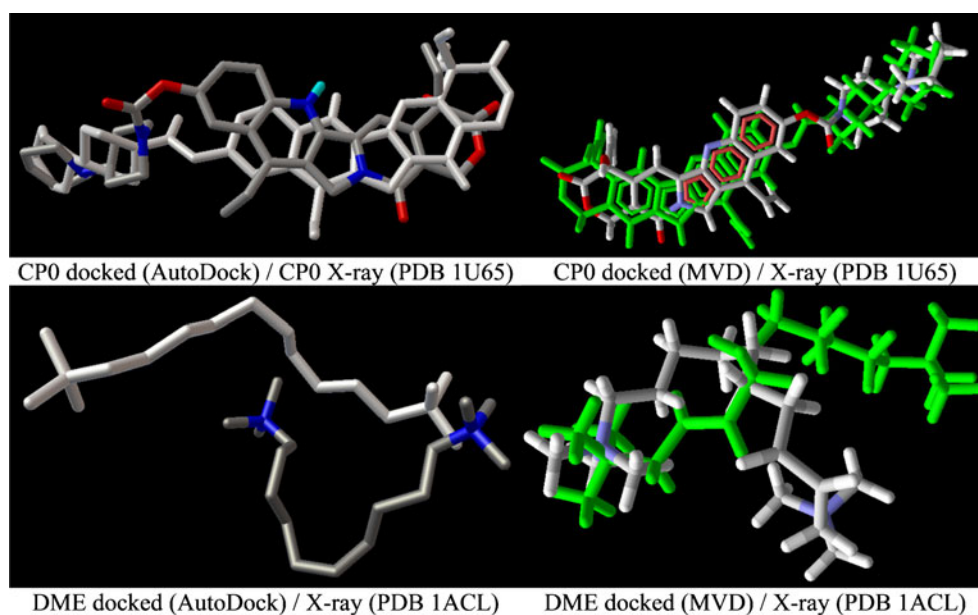


Table 2 Best docking poses (sorted by PDB ID) of the geissospermine (GSP) alkaloid into the *Torpedo californica* AChE binding site, comparing the results from the AutoDock (AutoDock score) and Molegro Virtual Docker (MolDock score and Re-Rank score) programs

AutoDock		Molegro Virtual Docker	
PDB ID ^a	Score	MolDock score	Re-Rank score
1ACJ	227.29	-169.28	-82.32
1ACL	95.93	-206.06	-104.33
1DX6	68.02	-197.14	-96.83
1E3Q	119.41	-190.38	-112.62
1EVE	77.15	-198.8	-86.66
1OCE	54.69	-221.73	-100.61
1U65	59.11	-206.88	-87.04
1VOT	59.13	-158.58	122.95
2ACE	69.45	-204.79	30.38
2ACK	125.57	-169.07	34.1

^a Italicized entries indicate the best results considering the three score values simultaneously

1EVE; MF2/1OCE; CP0/1U65; HUP/1VOT; ACH/2ACE; EDR/2ACK. This set of AChE active site ligands was chosen in order to span the molecular diversity of the ligands in terms of the number of rotatable bonds (nRotB ranging from zero to 12, Table 1) and molecular volume (CPK Vol ranging from 174 to 605 g mol⁻¹, Table 1. Each ligand was extracted from its original PDB X-ray structure and re-docked using both docking protocols.

The results showed that the RMSD values (Table 1) of the predicted and experimental poses (conformation and orientation) of the ligands into the binding pocket of AChE range from being slightly ($R=0.48$ AutoDock) to highly ($R=0.83$ MVD) correlated with the number of rotatable bonds (nRotB). For example, the complexes with the most rigid ligands, such as THA/1ACJ (THA, nRotB=0) and GNT/1DX6 (GNT, nRotB=1), usually showed the lowest RMSD values (<1.0 Å) for both docking protocols. On the other hand, the complexes with the most flexible ligands, such as EBW/1E3Q (EBW, nRotB=12) and MF2/1OCE (MF2, nRotB=10), showed the largest RMSD values (>3.0 Å).

However, in the AutoDock calculation, the EDR/2ACK complex showed the largest RMSD value (4.94 Å), in spite of its ligand having only two rotatable bonds, while the RMSD value was lower (0.84 Å) in the MVD calculation, showing a better performance. This result might be explained by the small molecular volume of its ligand (CPK Vol=196.19 Å³). In a relatively wide active site, such as that of AChE, the orientation search method included in AutoDock could not accurately reproduce the experimental coordinates of the ligand in this particular complex.

Comparing the covalently bound complexes, i.e., ACH/2ACE and MF2/1OCE, it is interesting to note that the ACH/2ACE (ACH, nRotB=4) complex had a RMSD value (1.14 Å) in the MVD calculations that was much lower than in AutoDock (4.43 Å), while the AutoDock (RMSD=4.77 Å) and MVD (RMSD=4.91 Å) protocols showed high RMSD values for the MF2/1OCE (MF2, nRotB=10) complex. In fact, it was expected that both protocols would show similar poor performances with ligands covalently bonded to the enzyme (i.e., the natural substrate acetylcholine and the MF268 irreversible inhibitor), since in these cases the “correct pose” (from the X-ray structure) is a forbidden solution.

Table 1 shows that five complexes calculated with MVD presented RMSDs of <1.0 Å (i.e., THA/1ACJ, HUP/1VOT, GNT/1DX6, EDR/2ACK, and E20/1EVE), while with AutoDock only two complexes had RMSDs of <1.0 Å (i.e., THA/1ACJ and GNT/1DX6). On the other hand, only three complexes calculated with MVD had RMSDs of >2.0 Å (i.e., MF2/1OCE, DME/1ACL, and EBW/1E3Q), while with AutoDock, five complexes had RMSDs of >2.0 Å (i.e., EDR/2ACK, ACH/2ACE, DME/1ACL, MF2/1OCE, and EBW/1E3Q). These results suggest that the MolDock algorithm is better parametrized, at least for this particular system, since it gave better performance results.

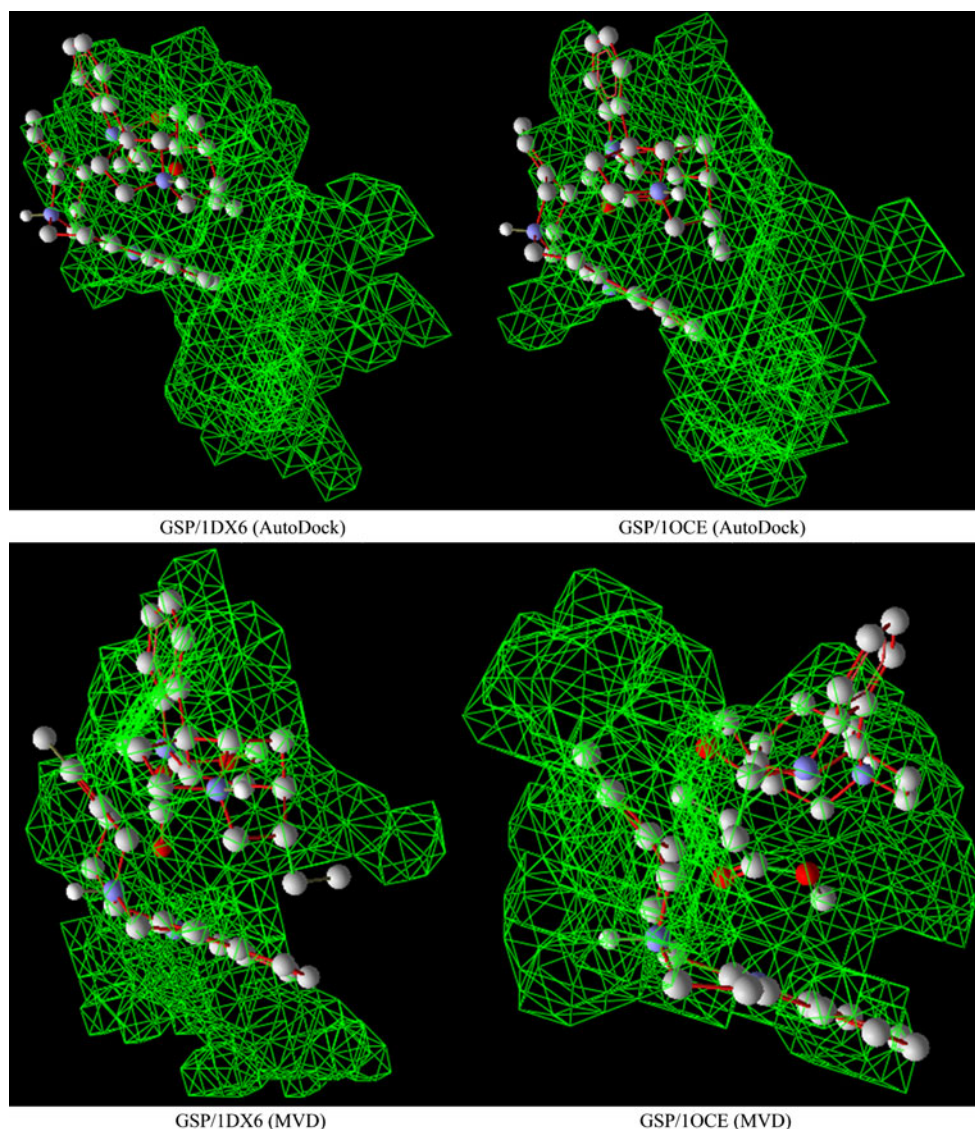
Overall, considering both protocols (AutoDock and MVD), the best results (RMSD values lower than 2.0 Å, Table 1) were obtained for ligands with no more than six rotatable bonds and CPK volumes that were greater than ~200 Å³. Therefore, these results suggest that the AutoDock and MVD simulations should accurately predict the conformation and binding orientation of GSP into the AChE binding site, since GSP has only four rotatable bonds and a relatively large volume (CPK volume ~600 Å³).

To further illustrate these results, we selected two complexes of the reversible inhibitors, CP0/1U65 (CP0, nRotB=6 and CPK Vol ~605 Å³) and DME/1ACL (DME, nRotB=11 and CPK Vol ~340 Å³) (Table 1), and simultaneously compared both criteria (nRotB and CPK Vol) with the RMSD results. The superpositions of the best docked poses of CP0 (AutoDock, RMSD=1.57 Å and MVD, RMSD=1.55 Å) and DME (AutoDock, RMSD=3.57 Å and MVD, RMSD=2.64 Å) with the corresponding bounded X-ray conformation are shown in Fig. 3.

AutoDock and MVD docking of GSP in the ten AChE X-ray structures

The CSD X-ray structure of GSP was used as the input ligand for docking simulations at the active sites of ten PDB X-ray structures of *TcAChE*, using the same protocols as those employed in the re-docking test. The 3D structure of each complex was scored using the AutoDock and MVD

Fig. 4 Graphical representations of the binding orientations of geissospermine (GSP) in the best GSP/1DX6 and GSP/1OCE solutions obtained via the AutoDock and Molegro Virtual Docker (MVD) programs. The *green grids* represent the cavity of the active site of AChE



(MolDock and Re-Rank) score functions. Choosing the best docked solution or pose (conformation and orientations) is often difficult, as results are particularly sensitive to the score function used in each particular docking program. Therefore, we adopted the criterion of the lowest docking energy in all cases.

In the docking simulations with AutoDock, the pose with the minimum AutoDock score value was selected as the best solution for each GSP/AChE complex (see Table S1 of the “[Electronic supplementary material](#)”). The AutoDock score values are calculated from the estimated free energy of binding (total), which is obtained from the following: $\text{total} = [(1) + (2) + (3) - (4)]$, where (1) is the final intermolecular energy, (2) is the final internal energy of the ligand, (3) is the torsional free energy, and (4) is the unbound system’s energy.

The docking analysis (Table S1) shows that the estimated free energy of binding is strongly dependent on

the final intermolecular energy and the final internal energy of the ligand. The variations in parameter values for the torsional free energy and the unbound system’s energy were almost negligible. The best results, according to a histogram analysis, were for the 1OCE, 1U65, 1VOT, 1DX6, and 2ACE complexes with GSP, which showed AutoDock score values (estimated free energy of binding) of 54.69, 59.11, 59.13, 68.02, and 69.45 kcal mol⁻¹, respectively (Table S1).

In the docking simulations with MVD, the pose with the minimum MolDock score value was selected as the best solution for each GSP/AChE complex (Table S2 of the “[Electronic supplementary material](#)”). In this case, the MolDock score is obtained from the sum of the total interaction energy and the internal energy of the ligand, i.e., $E_{\text{score}} = E_{\text{inter}} + E_{\text{intra}}$. Therefore, according to a histogram analysis, the best results were for the 1OCE, 1U65, 1ACL, 2ACE, 1EVE, and 1DX6 complexes with GSP, which

Table 3 Selected interatomic distances measured in the docking solutions of the GSP/1DX6 and GSP/IOCE complexes obtained by AutoDock and Molegro Virtual Docker (MVD)

Interatomic distances (Å)	AutoDock		MVD	
	1DX6	IOCE	1DX6	IOCE
AChE / GSP				
Tyr121-OH / N1	6.63	6.74	4.34	4.19
Phe331-O / N5	10.82	11.24	10.38	13.45
ASP72-Oδ2 / O20	7.08	8.97	7.01	7.94
Trp84-O / N33	9.20	9.40	8.83	8.88
Tyr334-OH / O68	7.80	10.55	6.38	5.53

showed MolDock score values of -221.73 , -206.88 , -206.06 , -204.79 , -198.80 , and -197.14 kcal mol $^{-1}$, respectively (Table S2).

Moreover, to increase the docking accuracy, the 100 best solutions obtained from 100 independent docking runs were re-ranked using the Re-Rank score function, which takes into account an sp^2 – sp^2 torsion term and a Lennard–Jones 12-6 potential. The Re-Rank score identifies the most promising docking solution from the solutions obtained by the docking algorithm (MolDock). Furthermore, docking experiments showed that a simple docking scoring function followed by a re-ranking procedure is adequate to identify high-quality binding modes in the place of more advanced scoring schemes [48]. After the re-ranking procedure, the new results showed a significant change in the order of the complexes (Table S2). Here, the best results, according to a histogram analysis, were for 1E3Q, 1ACL, IOCE, and 1DX6 complexes with GSP, which showed Re-Rank score values of -112.62 , -104.33 , -100.61 , and -96.83 kcal mol $^{-1}$, respectively (Table S2).

Overall, after considering the three scoring functions simultaneously, i.e., AutoDock score (Table S1), MolDock score and Re-Rank score (Table S2), in the consensus scoring scheme shown in Table 2 (a composite of Tables S1 and S2), we selected the GSP/1DX6 and GSP/IOCE complexes as the best solutions in the three scoring schemes for further analysis.

Analysis of the GSP/1DX6 and GSP/IOCE complexes from AutoDock and MVD

A priori, the GSP/IOCE complex should be excluded from this analysis, since in the validation test the MF2/IOCE complex showed high RMSD values in both docking methods (Table 1), probably due its high number of torsion angles ($n\text{RotB}=10$). Moreover, the MF2 ligand is covalently bonded to the enzyme in the X-ray MF2/IOCE complex, which may induce bias during the analysis of the

validation procedure. However, these features cannot influence the prediction results, because the docked ligand is not MF2 but GSP.

Therefore, we analyzed the pose solutions (conformation and orientation) of the GSP ligand in the GSP/1DX6 and GSP/IOCE complexes obtained with both docking methods (Fig. 4). In order to do so, we selected five heteroatoms from GSP and five heteroatoms from the residues located in the AChE binding site and measured the interatomic distances (Table 3) between ligand and enzyme using the LPC/CSU server.

Figure 4 shows that the ligand conformations in these complexes are similar, except for GSP/IOCE from MVD, since the variation between the interatomic distance O-Phe331 and N5-GSP in this complex and GSP/1DX6 (MVD) is the largest (Table 3). Moreover, the orientation of GSP inside the binding site is quite different when the AutoDock and MVD results are compared. In the GSP/1DX6 and GSP/IOCE complexes from AutoDock, GSP is closer to the border of the binding site (Fig. 4), while in the GSP/1DX6 and GSP/IOCE com-

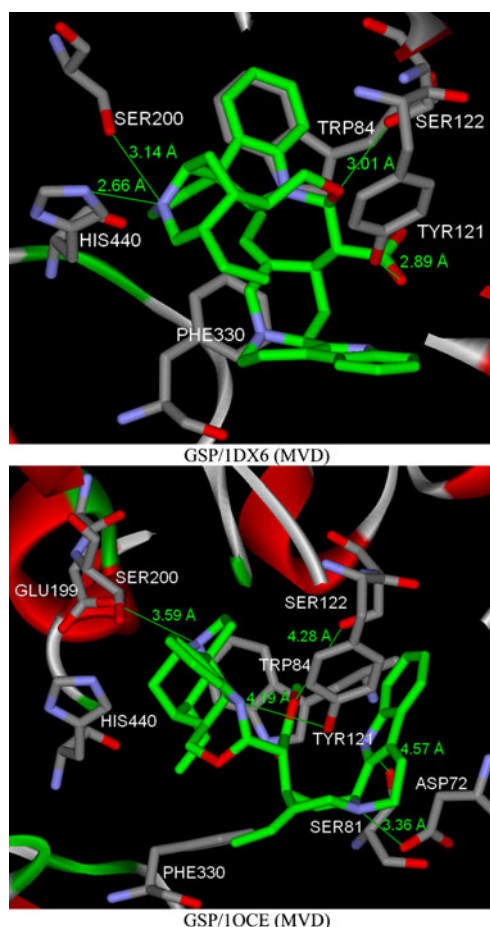


Fig. 5 Geissospermine (GSP) (carbon atoms in *green*) bonded to AChE (GSP/1DX6 and GSP/IOCE models), showing residues Trp84, Tyr121, Ser122, Ser200, Phe330, and His440

Table 4 Classification of the potential interaction types detected between each AChE ligand (including GSP) and AChE residues in the best docking pose solution from the Molegro Virtual Docker program, obtained using the LPC/CSU server

Ligand/AChE ^a	H-bonding ^b	Cation- π	π - π stacking	Hydrophobic	vdW ^c
GSP/1DX6	Tyr121 Ser122 Ser200 His440	nd	Trp84	Phe330	nd
GSP/IOCE	Asp72 Ser81 Tyr121 Ser122 Glu199	nd	nd	Phe330	Ser200 His440
THA/1ACJ	His440	nd	Trp84 Phe330	nd	nd
DME/1ACL	nd	Trp84 Trp279	nd	nd	Phe330
GNT/1DX6	Asp72 Glu199 Ser200	nd	nd	nd	Phe290
EBW/1E3Q	Tyr121	Trp279	nd	Phe330	His440
E20/1EVE	nd	Phe330	Trp84 Trp279	nd	Phe290 Phe331
MF2/IOCE	Tyr70 Gly118 Gly119 Ser200 His440	Trp279	nd	nd	nd
CP0/1U65	Phe284 Asp285	nd	Trp279	Trp84 Phe330	Phe331 Tyr334
HUP/1VOT	Tyr130 His440	Trp84 Phe330	nd	Gly118 Ser122	nd
ACH/2ACE	Ser200	Trp84 Phe330	nd	nd	His440
EDR/2ACK	Ser200 His440	Trp84	nd	Phe330 Phe331	nd

^a See text for ligand and AChE PDB codes; *GSP*, geissospermine; see Fig. S1 for structures of ligands: *THA*, tacrine; *DME*, decamethonium; *GNT*, (-)-galantamine; *EBW*, BW284C51; *E20*, E2020; *MF2*, MF268; *CP0*, CPT-11; *HUP*, (-)-huperzine A; *ACH*, acetylcholine; *EDR*, edrophonium; *nd*, not detected

^b Hydrogen-bonding interaction

^c van der Waals interaction

plexes from MVD, GSP is nearer to the center of the binding site (Fig. 4). Therefore, in order to analyze the interactions between GSP and the residues in AChE, we selected only the results from MVD, because in these complexes the ligand is nearer to the residues involved in AChE inhibition (Fig. 5).

Interactions between GSP and AChE in the GSP/1DX6 and GSP/IOCE complexes

We analyzed the interactions between GSP and the AChE residues in the GSP/1DX6 and GSP/IOCE complexes from MVD using the LPC/CSU server. These complexes showed several putative interactions between GSP and the residues of the AChE binding site (Fig. 5), including hydrogen bonding, π - π stacking, hydrophobic, and van der Waals, according to the classification of ligand-protein contacts by the LPC/CSU server.

In the GSP/1DX6 complex, at least four putative hydrogen-bonding interactions were detected between GSP and AChE: GSP-O68 and Tyr121-OH (O—O: $d=2.89$ Å); GSP-O20 and Ser122-OH (O—O: $d=3.01$ Å); GSP-N5 and Ser200-OH (N—O: $d=3.14$ Å); and GSP-N5 and His440-NH (N—N: $d=2.66$ Å). These specific interactions established a stable binding mode for the GSP/AChE complex, including interactions with one residue of the PAS (Tyr121) and two residues of the CT (Ser200 and His440).

In the GSP/IOCE complex, at least five putative hydrogen-bonding interactions were detected between the GSP and AChE: GSP-N33 and Asp72-CO₂H (N—O: $d=3.36$ Å); GSP-N27 and the carbonyl backbone of Ser81 (N—O: $d=4.57$ Å); GSP-N1 and Tyr121-OH (N—O: $d=4.19$ Å); GSP-O63 and Ser122-OH (O—O: $d=4.28$ Å); and GSP-N5 and Glu199-CO₂H (N—O: $d=3.59$ Å). These specific interactions established a stable binding mode for the GSP/AChE complex, including interactions with one

residue of the CAS (Glu199) and two residues of the PAS (Asp72 and Tyr121).

A π - π stacking (face-to-face aromatic-aromatic) interaction was detected between the GSP indole ring and Trp84 only for the GSP/1DX6 complex. This residue belongs to the CAS and is considered to be the main contributor to substrate stabilization at the active site of AChE. Molecular dynamic simulations of *Tc*AChE suggested that the conformational change of the Trp84 lateral chain could result in the appearance of a short channel that would allow the traffic of solvent, substrate or products [59, 60]. Therefore, the interaction of GSP with this residue would increase the blockade of the active site and at the same time make the GSP more tightly bound with the AChE.

A hydrophobic interaction was detected between GSP and Phe330 for both the GSP/1DX6 and the GSP/IOCE complexes. This residue belongs to the CAS and it is one of two aromatic residues that belong to the gorge bottleneck of the AChE binding site. It has been suggested that the orientation of its aromatic rings controls the opening/closing of the bottleneck [35]. We believe that its interactions with GSP could impair substrate access and contribute to AChE inhibition.

Finally, van der Waals interactions between GSP and important residues such as Ser200 and His440 (from the CT) were only detected for the GSP/IOCE complex.

Comparing the interactions between GSP and AChE in the GSP/1DX6 complex from MVD with those for the ten crystal structures of ligand/AChE complexes, we found that the GSP has some interactions in common with those of these ligands (Table 4). Among the hydrogen-bond interactions, at least one residue (i.e., Tyr121, Ser200 or His440) occurs in all of the complexes except those with DME, E20 and CP0 ligands. Among the π - π stacking interactions, only ligands THA and E20 interact with Trp84 as well as GSP. However, this residue undergoes cation- π (positively charged amine groups and π -systems) interactions with the ligands DME, HUP, ACH, and EDR. It seems that there is an interchange between π - π stacking and cation- π interactions, depending on the ligand. In relation to hydrophobic interactions, only three ligands (EBW, CP0, and EDR) showed interactions with Phe330, such as GSP.

An analogous comparison for the GSP/IOCE complex (Table 4) showed that among the hydrogen-bond interactions, at least one residue (i.e., Asp72, Glu199 or Tyr121) occurs in only two complexes with GNT and EBW ligands. In relation to hydrophobic interactions, the same behavior was observed as in the GSP/1DX6 complex. Concerning the van der Waals interactions, only His440 was detected in two complexes with EBD and ACH ligands.

Analyzing the occurrences of common residues independent of the interaction type, and comparing GSP/1DX6

and the other ten complexes (Table 4), at least two residues are seen to occur in all ligands, except for the GNT ligand, which has just one residue in common (Ser200). The frequencies are: four (HUP, ACH, and EDR), three (THA and EBW), and two (DME, E20, MF2, and CP0) residues in common with GSP/1DX6. However, upon comparing GSP/IOCE and the other ten complexes (Table 4), at least two residues occur in all ligands, except for E20 (Phe330), CP0 (Phe330), and DME (Phe330). The frequencies are: three (ACH, EBW, EDR, GNT, and HUP) and two (MF2 and THA) residues in common with GSP/IOCE.

Overall, we selected the GSP/1DX6 complex as the best solution because it shows more common putative interactions with the ten ligands. Moreover, the four hydrogen bonds in this complex could be classified as moderate (2.5–3.2 Å) [61]. In the GSP/IOCE complex, two hydrogen bonds could be classified as weak (3.2–4.0 Å) [61], and the other three are far from this maximum distance criterion. In addition, only the GSP/1DX6 complex shows a π - π stacking interaction, while in the GSP/IOCE complex neither π - π stacking nor cation- π interactions were detected; depending on the ligand (except GNT), there is at least one of these interactions. Therefore, we recommend the GSP/1DX6 complex for further studies of molecular modification strategies, such as molecular simplification and isosteric replacement.

Conclusions

In this work, we docked the alkaloid geissospermine (GSP) into the active site of acetylcholinesterase (AChE) in order to predict its putative “bioactive” conformation and binding orientation, since this natural product is an AChE inhibitor. Several docking calculations were carried out using the AutoDock and Molegro Virtual Docker (MVD) programs.

The best docking solution (GSP/1DX6 complex) was obtained using MVD, which showed a preferential binding mode between specific groups of GSP and the AChE residues. In this complex, some putative ligand/protein interactions, such as hydrogen bonds, π - π stacking, and hydrophobic interactions were detected. Hydrogen bonding interactions with Ser200 and His440 were detected, which may suggest the influence of the catalytic triad in the AChE inhibition mechanism by GSP.

This study provides the basis to propose structural changes to the GSP structure, such as molecular simplification and isosteric replacement, which would aid the design of new potential AChE inhibitors relevant to the treatment of Alzheimer’s disease.

Acknowledgments We gratefully acknowledge the financial support provided by Brazilian governmental agencies: CNPq (Conselho Nacional de Desenvolvimento Científico e Tecnológico), CAPES (Coordenação de Aperfeiçoamento de Pessoal de Nível Superior), and FAPERJ (Fundação de Amparo à Pesquisa do Estado do Rio de Janeiro).

References

- Alcala MDM, Vivas NM, Hospital S, Camps P, Munoz-Torrero D, Badia A (2003) Characterisation of the anticholinesterase activity of two new tacrine-huperzine A hybrids. *Neuropharmacol* 44:749–755
- Cutler NR, Sramek JJ (2001) Review of the next generation of Alzheimer's disease therapeutics: challenges for drug development. *Prog Neuro-Psychopharmacol Biol Psychiatry* 25:27–57
- Ginsberg SD, Che S, Counts SE, Mufson EJ (2006) Single cell gene expression profiling in Alzheimer's disease. *NeuroRx* 3:302–318
- Bertram L, Busch R, Spiegl M, Lautenschlager NT, Muller U, Kurz A (1998) Paternal age is a risk factor for Alzheimer disease in the absence of a major gene. *Neurogenet* 1:277–280
- Tsai MS, Tangalos EG, Petersen RC, Smith GE, Schaid DJ, Kokmen E, Ivnik RJ, Thibodeau SN (1994) Apolipoprotein-E: risk factor for Alzheimer-disease. *Am J Hum Genet* 54:643–649
- Fleminger S (2003) Head injury as a risk factor for Alzheimer's disease. *J Neurol Neurosurg Psychiatry* 74:857–862
- Martins IJ, Hone E, Foster JK, Sunram-Lea SI, Gnjec A, Fuller SJ, Nolan D, Gandy SE, Martins RN (2006) Apolipoprotein E, cholesterol metabolism, diabetes, and the convergence of risk factors for Alzheimer's disease and cardiovascular disease. *Mol Psychiatry* 11:721–736
- Kivipelto M, Laakso MP, Tuomilehto J, Nissinen A, Soininen H (2002) Hypertension and hypercholesterolaemia as risk factors for Alzheimer's disease—potential for pharmacological intervention. *CNS Drugs* 16:435–444
- Kivipelto M, Solomon A (2006) Cholesterol as a risk factor for Alzheimer's disease—epidemiological evidence. *Acta Neurol Scand* 114:50–57
- De la Torre JC (2006) How do heart disease and stroke become risk factors for Alzheimer's disease? *Neurol Res* 28:637–644
- Anstey KJ, von Sanden C, Salim A, O'Kearney R (2007) Smoking as a risk factor for dementia and cognitive decline: a meta-analysis of prospective studies. *Am J Epidemiol* 166:367–378
- Mebane-Sims I (2009) 2009 Alzheimer's disease facts and figures. *Alzheimers Dementia* 5:234–270
- Schmidt R, Assem-Hilger E, Benke T, Dal-Bianco P, Delazer M, Ladurner G, Jellinger K, Marksteiner J, Ransmayr G, Schmidt H, Stögmann E, Wancata J, Wehringer C (2008) Sex differences in Alzheimer's disease. *Neuropsychiatrie* 22:1–15
- Hebert LE, Scherr PA, McCann JJ, Beckett LA, Evans DA (2001) Is the risk of developing Alzheimer's disease greater for women than for men? *Am J Epidemiol* 153:132–136
- Patwardhan MB, McCrory DC, Matchar DB, Samsa GP, Rutschmann OT (2004) Alzheimer disease: operating characteristics of PET—a meta-analysis. *Radiol* 273:73–80
- Mohs RC (2005) The clinical syndrome of Alzheimer's disease: aspects particularly relevant to clinical trials. *Genes Brain Behavior* 4:129–133
- Brookmeyer R, Johnson E, Ziegler-Graham K, Arrighi HM (2007) Forecasting the global burden of Alzheimer's disease. *Alzheimers Dementia* 3:186–191
- Scarpini E, Scheltens P, Feldman H (2003) Treatment of Alzheimer's disease: current status and new perspectives. *Lancet Neurol* 2:539–547
- Bartus RT, Dean RL, Beer B, Lippa AS (1982) The cholinergic hypothesis of geriatric memory dysfunction. *Science* 217:408–417
- Francis PT, Palmer AM, Snape M, Wilcock GK (1999) The cholinergic hypothesis of Alzheimer's disease: a review of progress. *J Neurol Neurosurg Psychiatry* 66:137–147
- Cummings JL, Kaufer D (1996) Neuropsychiatric aspects of Alzheimer's disease: the cholinergic hypothesis revisited. *Neurol* 47:876–883
- Perry EK (1986) The cholinergic hypothesis—10 years on. *Br Med Bull* 42:63–69
- Lleo A, Greenberg SM, Growdon JH (2006) Current pharmacotherapy for Alzheimer's disease. *Annu Rev Med* 57:513–533
- von Eschenbach AC (2007) Alzheimer's disease: FDA's role in new product development. <http://www.fda.gov/NewsEvents/Testimony/ucm110879.htm>. Accessed September 2010
- Farlow MR, Cummings JL (2007) Effective pharmacologic management of Alzheimer's disease. *Am J Med* 120:388–397
- Cummings JL (2000) Cholinesterase inhibitors: a new class of psychotropic compounds. *Am J Psychiatry* 157:4–15
- Rogers SL, Farlow MR, Doody RS, Mohs R, Friedhoff LT, Alcala B, Baumel B, Booker G, Dexter J, Farmer M, Feighner JP, Ferris S, Gordon B, Gorman DG, Hanna G, Harrell LE, Hubbard R, Kennedy J, McCarthy J, Scharre DW, Schaerf F, Schneider L, Seltzer B, Siegel A, Stark SR, Strauss A, Walshe TM (1998) A 24-week, double-blind, placebo-controlled trial of donepezil in patients with Alzheimer's disease. *Neurol* 50:136–145
- Tariot PN, Solomon PR, Morris JC, Kershaw P, Lilienfeld S, Ding C (2000) A 5-month, randomized, placebo-controlled trial of galantamine in AD. *Neurol* 54:2269–2276
- Findeis MA (2007) The role of amyloid beta peptide 42 in Alzheimer's disease. *Pharmacol Ther* 116:266–286
- Shen LL, Liu GX, Tang Y (2007) Molecular docking and 3D-QSAR studies of 2-substituted 1-indanone derivatives as acetylcholinesterase inhibitors. *Acta Pharmacol Sin* 28:2053–2063
- Marco-Contelles J, Carreiras MD, Rodriguez C, Villarroya M, Garcia AG (2006) Synthesis and pharmacology of galantamine. *Chem Rev* 106:116–133
- Sugimoto H, Yamanishi Y, Iimura Y, Kawakami Y (2000) Donepezil hydrochloride (E2020) and other acetylcholinesterase inhibitors. *Curr Med Chem* 7:303–339
- Lima JA (2005) Isolamento e Identificação da Geissospermina, o Alcalóide Responsável pela Atividade Anticolinesterásica do Extrato do *Geissospermum vellozii* (thesis). Universidade Federal do Rio de Janeiro, Rio de Janeiro
- Lima JA, Costa RS, Epifânio RA, Castro NG, Rocha MS, Pinto AC (2009) *Geissospermum vellozii* stem bark: anticholinesterase activity and improvement of scopolamine-induced memory deficits. *Pharmacol Biochem Behavior* 92:508–513
- Xu YC, Colletier JP, Weik M, Jiang HL, Moulton J, Silman I, Sussman JL (2008) Flexibility of aromatic residues in the active-site gorge of acetylcholinesterase: X-ray versus molecular dynamics. *Biophys J* 95:2500–2511
- Kryger G, Silman I, Sussman JL (1998) Three-dimensional structure of a complex of E2020 with acetylcholinesterase from *Torpedo californica*. *J Physiol Paris* 92:191–194
- Berman HM, Westbrook J, Feng Z, Gilliland G, Bhat TN, Weissig H, Shindyalov IN, Bourne PE (2000) The Protein Data Bank. *Nucleic Acids Res* 28:235–242
- Harel M, Schalk I, Ehretsabatier L, Bouet F, Goeldner M, Hirth C, Axelsen PH, Silman I, Sussman JL (1993) Quaternary ligand-binding to aromatic residues in the active-site gorge of acetylcholinesterase. *Proc Natl Acad Sci USA* 90:9031–9035

39. Greenblatt HM, Kryger G, Lewis T, Silman I, Sussman JL (1999) Structure of acetylcholinesterase complexed with (–)-galanthamine at 2.3 angstrom resolution. *FEBS Lett* 463:321–326
40. Felder CE, Harel M, Silman I, Sussman JL (2002) Structure of a complex of the potent and specific inhibitor BW284C51 with *Torpedo californica* acetylcholinesterase. *Acta Crystallogr Sect D* 58:1765–1771
41. Kryger G, Silman I, Sussman JL (1999) Structure of acetylcholinesterase complexed with E2020 (Aricept®): implications for the design of new anti-Alzheimer drugs. *Structure* 7:297–307
42. Bartolucci C, Perola E, Cellai L, Brufani M, Lamba D (1999) “Back door” opening implied by the crystal structure of a carbamoylated acetylcholinesterase. *Biochem* 38:5714–5719
43. Harel M, Hyatt JL, Brumshtein B, Morton CL, Yoon KJP, Wadkins RM, Silman I, Sussman JL, Potter PM (2005) The crystal structure of the complex of the anticancer prodrug 7-ethyl-10-[4-(1-piperidino)-1-piperidino]carbonyloxycamptothecin (CPT-11) with *Torpedo californica* acetylcholinesterase provides a molecular explanation for its cholinergic action. *Mol Pharmacol* 67:1874–1881
44. Raves ML, Harel M, Pang YP, Silman I, Kozikowski AP, Sussman JL (1997) Structure of acetylcholinesterase complexed with the nootropic alkaloid, (–)-huperzine A. *Nat Struct Biol* 4:57–63
45. Ravelli RBG, Raves ML, Ren Z, Bourgeois D, Roth M, Kroon J, Silman I, Sussman JL (1998) Static Laue diffraction studies on acetylcholinesterase. *Acta Crystallogr Sect D* 54:1359–1366
46. ACD/Labs (2009) ACD/ChemSketch Freeware, version 12.00. Advanced Chemistry Development, Inc., Toronto
47. Chiaroni A, Riche C (1979) Structure and stereochemistry of indole alkaloids. 5. Structure of geissospermine. *Acta Crystallogr Sect B* 35:1820–1825
48. Allen FH (2002) The Cambridge Structural Database: a quarter of a million crystal structures and rising. *Acta Crystallogr Sect B* 58:380–388
49. Tripos Inc. (2008) Website. <http://tripos.com/>
50. Gasteiger J, Marsili M (1980) Iterative partial equalization of orbital electronegativity—a rapid access to atomic charges. *Tetrahedron* 36:3219–3228
51. Clark M, Cramer RD, Vanopdenbosch N (1989) Validation of the general-purpose Tripos 5.2 force-field. *J Comput Chem* 10:982–1012
52. Morris GM, Goodsell DS, Halliday RS, Huey R, Hart WE, Belew RK, Olson AJ (1998) Automated docking using a Lamarckian genetic algorithm and an empirical binding free energy function. *J Comput Chem* 19:1639–1662
53. Thomsen R, Christensen MH (2006) MolDock: a new technique for high-accuracy molecular docking. *J Med Chem* 49:3315–3321
54. Teixeira C, Barbault F, Rebehmed J, Liu K, Xie L, Lu H, Jiang S, Fan B, Maurel F (2008) Molecular modeling studies of *N*-substituted pyrrole derivatives—potential HIV-1 gp41 inhibitors. *Bioorg Med Chem* 16:3039–3048
55. Mashhadi HR, Shanечи HM, Lucas C (2003) A new genetic algorithm with Lamarckian individual learning for generation scheduling. *IEEE Trans Power Syst* 18:1181–1186
56. Sobolev V, Sorokine A, Prilusky J, Abola EE, Edelman M (1999) Automated analysis of interatomic contacts in proteins. *Bioinf* 15:327–332
57. Storn R, Price K (1997) Differential evolution—a simple and efficient heuristic for global optimization over continuous spaces. *J Global Optim* 11:341–359
58. Thomsen R (2003) Flexible ligand docking using differential evolution. In: 2003 Congr on Evolutionary Computation, Canberra, Australia, 8–12 Dec 2003, pp 2354–2361
59. Gilson MK, Straatsma TP, McCammon JA, Ripoll DR, Faerman CH, Axelsen PH, Silman I, Sussman JL (1994) Open “back door” in a molecular-dynamics simulation of acetylcholinesterase. *Science* 263:1276–1278
60. Axelsen PH, Harel M, Silman I, Sussman JL (1994) Structure and dynamics of the active-site gorge of acetylcholinesterase—synergistic use of molecular-dynamics simulation and X-ray crystallography. *Protein Sci* 3:188–197
61. Jeffrey GA (1997) An introduction to hydrogen bonding. Oxford University Press, New York